Imaging of Percolative Conduction Paths and Their Breakdown in Phase-Separated $(La_{1-y}Pr_y)_{0.7}Ca_{0.3}MnO_3$ with $y = 0.7$

M. Tokunaga,* Y. Tokunaga, and T. Tamegai

Department of Applied Physics, The University of Tokyo, 7-3-1 Hongo, Bunkyo-ku, Tokyo 113-8656, Japan

(Received 10 February 2004; published 15 July 2004)

Local magnetization and current distribution in $(La_{1-y}Pr_y)_{0.7}Ca_{0.3}MnO_3$ ($y = 0.7$) crystals are studied by a magneto-optical (MO) imaging technique. MO images below 120 K visualize inhomogeneous magnetization and conduction paths that manifest the percolative conduction originated from the mesoscopic phase separation into ferromagnetic metals and antiferromagnetic insulators. Application of large amounts of current switches the current distribution from inhomogeneous to homogeneous concomitantly with a steep increase in resistivity. These phenomena are discussed in view of current induced collapse of the phase separation through a local heating.

DOI: 10.1103/PhysRevLett.93.037203 PACS numbers: 75.47.Lx, 64.60.Ak, 64.75.+g, 71.30.+h

In condensed matter physics, studies of the boundary region between two competing phases provide insights into the nature of the adjacent phases. In addition, competing orders help to cause prominent change in the physical properties by small perturbation, e.g., the colossal magnetoresistance effect [1]. Recent experimental studies with high spatial resolution revealed the presence of electronic inhomogeneity in this boundary region even in the best-quality samples available at present [2–6]. Theoretical studies revealed a crucial role of randomness in the vicinity of the multicritical point [7–9]. Although it is still controversial whether the origin of the *colossal* response for external perturbation is static phase separation (PS) or dynamic fluctuation, the existence of the PS in high-quality crystals is widely accepted as an intrinsic nature due to the presence of the quenched disorder that is inherent to many compounds. In manganites, static PS into ferromagnetic metal and antiferromagnetic insulator results in percolative conduction, and can cause an anomalous magnetoresistance effect [1] and fluctuating conduction [10].

Experimentally observed PS can be categorized into two classes: microscopic (nanometer scale) and mesoscopic (micrometer scale). In many transition-metal oxides, tuning carrier concentration causes changes in the ground state. PS in such materials can consist of domains of competing phases with different carrier density. Consequently, Coulomb interaction restricts the size of the domains, typically in nanometer scale. On the other hand, a manganite with perovskite-type structure $(La_{1-y}Pr_y)_{1-x}Ca_xMnO_3$ ($x \approx 0.3$) changes ground state property without changing carrier density. The end members $La_{1-x}Ca_xMnO_3$ and $Pr_{1-x}Ca_xMnO_3$ show different magnetic and electronic properties in their ground states: ferromagnetic metal and antiferromagnetic charge-ordered insulator at the same doping levels of $0.3 \leq x < 0.5$ [11,12]. In such a system, domains in the PS states are expected to grow without any cost of the Coulomb energy. Indeed mesoscopic PS in thin samples has been directly visualized by experiments of electron and magnetic force microscopy through detection of local magnetization or superlattice spots of charge ordering [2,3,13–15]. In crystals, however, almost no such real space images have been reported while it is indispensable to consider the mesoscopic PS as a nature of bulk materials.

In this study, we performed real space imaging of local magnetization and current distribution in crystals of $(La_{1-y}Pr_y)_{0.7}Ca_{0.3}MnO_3$ ($y = 0.7$: LPCMO-0.7) by a magneto-optical imaging technique. We chose this material because powder neutron diffraction measurement showed mesoscopic (≥ 1000 Å) PS in this composition [16]. We have successfully visualized percolative conduction paths for the first time in addition to inhomogeneous magnetization in mesoscopic PS states.

Crystals of LPCMO-0.7 are grown by the floating-zone method. The synthesized rods are cut into long strips. X-ray diffraction measurement on powder taken from the adjacent part of the crystal to the strips shows no traces of any secondary phase. Optically flat surfaces for observation are achieved by mechanical polishing and subsequent Ar-ion milling with cooling by liquid nitrogen to remove strain at the surface. Results shown in this Letter are for a sample with dimensions of 3100 μm $\times$ 350 μm $\times$ 150 μm. We performed similar experiments on two other samples with the same composition and confirmed qualitatively similar results to those reported here. The present sample contains several crystallographic domains as shown in polarizing microscope image of Fig. 1(a). However, these domains are larger than 100 μm and show no correlation with the inhomogeneity focused in this study.

Magneto-optical (MO) imaging is the method that visualizes local magnetic fields perpendicular to the sample surface using a garnet indicator film mounted on the sample. Polarized light passed through the garnet is reflected at a mirror located between the garnet and the sample. Change in polarization due to Faraday rotation

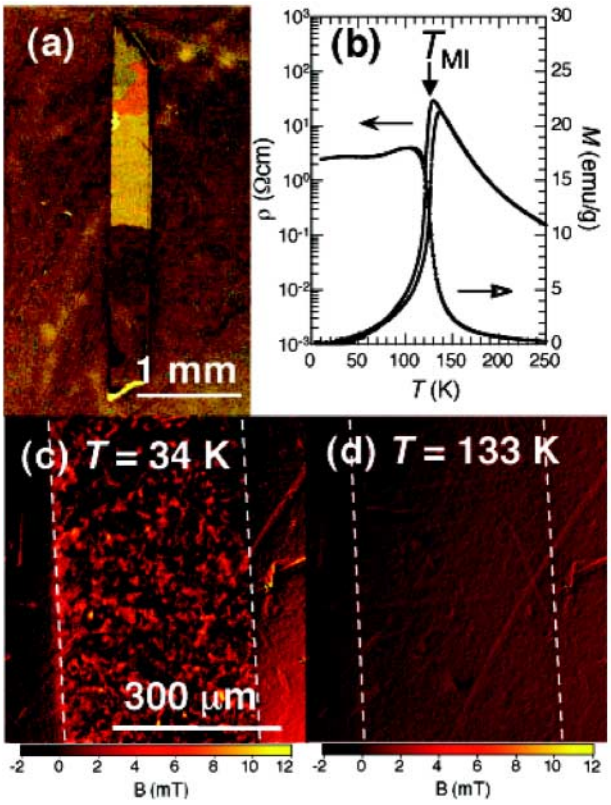

FIG. 1 (color online). (a) A polarizing microscope image of the observed surface. Areas with different color correspond to different crystallographic domains. (b) Temperature dependence of resistivity and average magnetization in heating and cooling processes. MO images without current at (c) 34 K and (d) 133 K. Dashed lines represent edges of the sample.

caused by stray fields from the sample to the garnet is visualized by a polarizing microscope and captured by a cooled charge-coupled device camera. Since the sample is not directly irradiated with the light, we do not expect any photoinduced effects to the electronic states in the sample [17]. Our present experimental system can visualize local magnetic fields at spatial resolution of several micrometers with a sensitivity better than 10 μT by a use of a differential method [18,19].

The sample and the indicator film are set at the top of a cold finger connected to a closed-cycle helium refrigerator [20]. Temperature (T) shown in this Letter is the value monitored at the top of the cold finger. Resistivity is measured by a standard four-probe method. Good electrical contacts are formed by silver paste with heat treatment. The average magnetization over the sample is measured by commercial superconducting quantum interference device magnetometer (MPMS-XL, quantum design).

Figure 1(b) is the temperature dependence of resistivity (ρ) at a constant current of 10 μA and average magnetization over the sample (M). The magnetization is measured in magnetic fields of 0.1 T. This sample becomes metallic and shows ferromagnetic component below about 125 K, which is defined as the transition temperature T_{MI}. Figures 1(c) and 1(d) show MO images at around the center of the sample at 34 and 133 K, respectively. Dashed lines are drawn to indicate the edges of the sample. The light gray (yellow) and black region corresponds to the area with large and small magnetization perpendicular to the surface. Comparison between (c) and (d) shows inhomogeneous magnetization at 34 K in addition to temperature independent noise caused mainly by scratches in the indicator. In Fig. 1(c), observed inhomogeneous magnetization is an average over the spatial resolution of several micrometers, so it cannot be nanoscale PS that will be averaged out in this scale. This inhomogeneity only appears below the T_{MI}. Taking the results of neutron diffraction into account [16], this magnetic inhomogeneity can be ascribed to mesoscopic PS into ferromagnetic and antiferromagnetic domains.

We studied current distribution in this sample through observations of magnetic fields caused by the current. Contribution of the current to the MO image appears in differential images between positive and negative current. Thus obtained differential images are shown in Figs. 2(a), 2(c), and 2(d) after averaging over 450 sets of differential images (takes about 2 min in total for each image) to achieve better contrast. Average current direction is shown by an arrow in Fig. 2(a). At $T = 33$ K, field distribution caused by the current appears to be inhomogeneous. We do not consider this inhomogeneity as current-induced flop of magnetic domains, because no such features appear in magnetization distribution before and after injection of a current of 15 mA as will be seen in Fig. 4(b). On the assumption that current component normal to the surface is zero inside the sample, we calculate the current distribution following the method reported in Ref. [21]. Although this assumption cannot be justified in this sample in a strict sense, it is helpful to visualize inhomogeneous current distribution at $T = 33$ K as shown in Fig. 2(b). This inhomogeneity appears static at least over several tens of minutes.

An increase of temperature above T_{MI}, however, changes the current distribution to homogeneous. Figure 2(c) is the differential image for $I = \pm 15$ mA at 146 K. This image is a typical result for uniform current that causes positive and negative field at the edge of the sample. This change indicates that inhomogeneous conduction at low temperatures corresponds neither to chemical inhomogeneity nor structural defects, which cannot be removed with an increase of temperature to 146 K.

Application of a larger current also breaks the inhomogeneous conduction. Figure 2(d) shows a differential MO image between $I = \pm 25$ mA at 33 K. The homogeneous image shows remarkable contrast with that for $I = \pm 15$ mA. We performed MO imaging at various values of currents at $T = 33$ K and found that this change occurs drastically. Images for currents $|I| \leq 15$ mA show almost

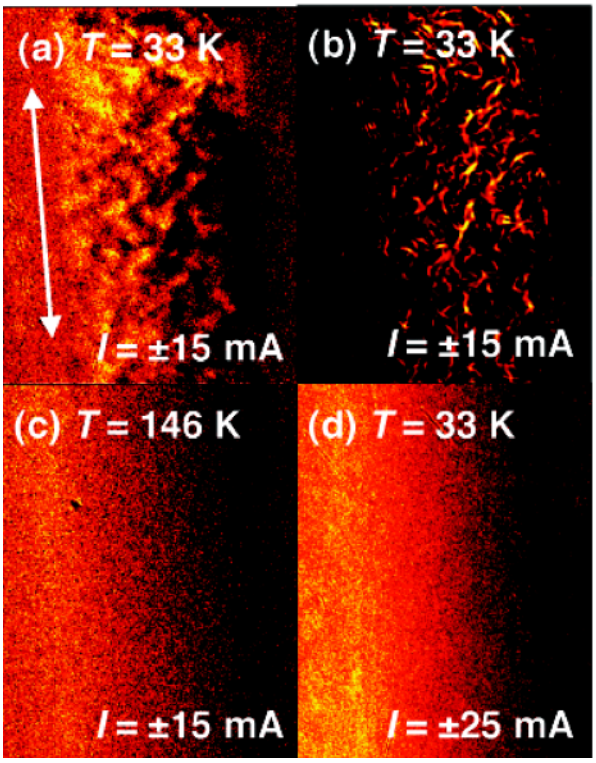

FIG. 2 (color online). (a) Differential MO image for $I = \pm 15$ mA at $T = 33$ K. Bright and dark parts correspond to the regions with positive and negative magnetic field caused by the current. The direction of the average current is shown by an arrow. (b) Current distribution calculated from magnetic image of (a). The light gray (yellow) region corresponds to the area where amplitude of the current is large. (c) Differential MO image for $I = \pm 15$ mA at $T = 146$ K. (d) Differential MO image for $I = \pm 25$ mA at $T = 33$ K.

similar inhomogeneous patterns to Fig. 2(a), whereas those for $|I| \geq 20$ mA shows homogeneous as in Fig. 2(d).

To clarify the origin of the change in current distribution, we studied voltage-current (V-I) characteristics at various temperatures from 33 to 146 K [Fig. 3(a)]. At 33 K, an increase of the current breaks ohmic relation at 16 mA and causes a steep increase in voltage, i.e., an increase in resistivity, more than 3 orders of magnitude (see inset). A decrease of I from 30 mA causes a drop of V to the ohmic state at around 4 mA accompanied by a hysteresis. A subsequent sweep to negative I shows an antisymmetric V-I curve with respect to the origin. This fact indicates the reproducibility of the V-I characteristics. The threshold current (I_{th}) decreases as temperature increases and is hardly identified above T_{MI}. Thereby, the abrupt change in the V-I curves is a character in the PS state. Such an effect reminds us of the electric field induced collapse of charge ordering [22]. In the present case, however, induced phase has higher resistivity indicating that the mechanism is different.

As can be expected from the V-I curves, removal of a current larger than I_{th} reconstructs the inhomogeneous

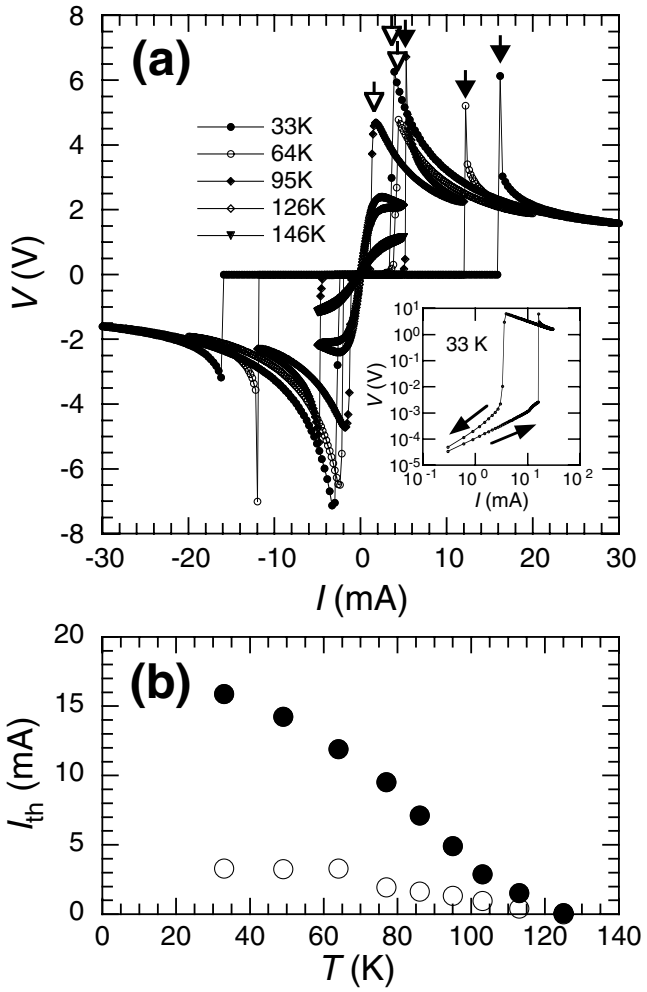

FIG. 3. (a) V-I curves at various temperatures between 33 and 146 K. The inset shows the V-I curve at 33 K in logarithmic scale. (b) Temperature dependence of the threshold current I_{th} in current up (closed circles) and down (open circles) procedures defined as marked by closed and open arrows in (a).

metallic state. To check whether this secondary state is the same with the primary one or not, we take differential MO images between before and after the application of temporal current I_{temp} with a duration time of 2 s at 33 K. All the images are taken at $I = 0$ so that the observed image comes only from magnetization of the sample. Figure 4(a) shows the differential image for $I_{\mathrm{temp}} = 25$ mA ($> I_{\mathrm{th}}$). The existence of contrast represents that the secondary state is different from the primary one. This fact indicates that the pattern of the phase separation is not fixed in the crystal but changes with the process to reach it. The image for $I_{\mathrm{temp}} = 25$ mA [Fig. 4(a)] is in contrast to that for $I_{\mathrm{temp}} = 15$ mA ($< I_{\mathrm{th}}$) [Fig. 4(b)], where temporal current does not modify the PS pattern.

Let us discuss the origin of the change caused by the current. As shown in Figs. 1(c) and 2(a), this sample is in a PS state and shows percolative conduction below T_{MI}. In this state, transport currents should be concentrated to metallic channels. Since the states with $I \geq I_{\mathrm{th}}$ has higher

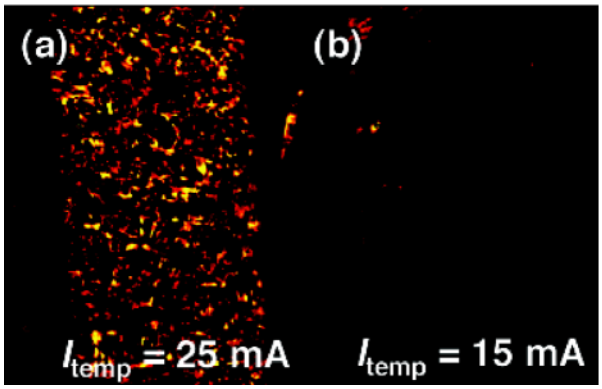

FIG. 4 (color online). Differential MO images at 33 K and $I = 0$ A between before and after application of temporal current I_{temp} of (a) 25 mA and (b) 15 mA.

resistivity, observed change by a current can be ascribed to the collapse of these metallic channels. The application of large amounts of current raises the temperature of the metallic paths by local heating, and changes to insulating from the region where metallicity is weaker than the others. Under a constant current condition, closure of a metallic channel forces the current to flow into the remaining channels, and thus stimulates further local heating. As a result, all the conduction paths will be closed almost at once. In a related material $La_{5/8-y}Pr_yCa_{3/8}MnO_3$, Kiryukhin *et al.* reported the coexistence of two insulating (charge-ordered and charge-disordered) phases above T_{MI} [23], where we observed homogeneous images. These two sets of results are not necessarily inconsistent with each other. Changes in contrast detected by the differential MO method depend on sizes and the resistivity ratio of the coexisting domains. According to the specific heat data of $La_{5/8-y}Pr_yCa_{3/8}MnO_3$ [23], energy required to heat the sample from 30 to 125 K is estimated to 27 mJ in adiabatic condition. In the present study, the power introduced by the current up to the I_{th} reaches about 40 mJ for $T = 30$ K, and likely can cause such a change.

The present studies on crystals show similar results to those reported for thin samples [3,15], so that mesoscopic PS is a nature of bulk material in this system. According to the phase diagram of $(La_{1-y}Pr_y)_{0.7}Ca_{0.3}MnO_3$ determined by powder neutron diffraction [16], this system can be classified into those with strong disorder (see Refs. [24,25]). Mesoscopic PS has also been reported in Cr-doped $Nd_{0.5}Ca_{0.5}MnO_3$ and $Pr_{0.5}Ca_{0.5}MnO_3$ [13,14,26,27]. In these materials, doped Cr ions are regarded as fixed hole sites that can strongly disturb the charge ordering in the matrix. Our observation indicates that in manganites with strong disorder, which does not originate from impurities or stress from the substrates but inherent in compounds, mesoscopic PS really exists as a nature of bulk materials. Even though it is strong, the disorder does not fix the PS pattern in the same location as shown in Fig. 4(a).

In conclusion, we visualized inhomogeneous magnetization and current distribution in crystals of phase-separated $(La_{1-y}Pr_y)_{0.7}Ca_{0.3}MnO_3$ ($y = 0.7$). The results indicate that mesoscopic phase separation is an intrinsic nature in a bulk material in this manganite. We observed the collapse of the percolative conduction in the phase-separated state by the application of a current larger than a threshold value.

The authors thank E. Zeldov and R. J. Wijngaarden for help in current visualization by magneto-optical imaging. This work is supported by Grant-in-aid for Scientific Research from the Ministry of Education, Culture, Sports, Science and Technology.

*Electronic address: mtokunaga@ap.t.u-tokyo.ac.jp

[1] For a review, see *Colossal Magnetoresistance, Charge Ordering and Related Properties of Manganese Oxides*, edited by C. N. R. Rao and B. Raveau (World Scientific, Singapore, 1998).
[2] S. Mori, C. H. Chen, and S. -W. Cheong, Phys. Rev. Lett. **81**, 3972 (1998).
[3] M. Uehara *et al.*, Nature (London) **399**, 560 (1999).
[4] M. Fäth *et al.*, Science **285**, 1540 (1999).
[5] S. H. Pan *et al.*, Nature (London) **413**, 282 (2001).
[6] I. Iguchi, T. Yamaguchi, and A. Sugimoto, Nature (London) **412**, 420 (2001).
[7] E. Dagotto, Phys. Rep. **344**, 1 (2001), and references therein.
[8] S. Murakami and N. Nagaosa, Phys. Rev. Lett. **90**, 197201 (2003).
[9] Y. Motome, N. Furukawa, and N. Nagaosa, Phys. Rev. Lett. **91**, 167204 (2003).
[10] R. D. Merithew *et al.*, Phys. Rev. Lett. **84**, 3442 (2000).
[11] P. Schiffer *et al.*, Phys. Rev. Lett. **75**, 3336 (1995).
[12] Y. Tomioka *et al.*, Phys. Rev. B **53**, 1689 (1996).
[13] H. Oshima *et al.* Phys. Rev. B **63**, 094420 (2001).
[14] S. Mori *et al.*, J. Phys. Soc. Jpn. **71**, 1280 (2002).
[15] L. Zhang *et al.*, Science **298**, 805 (2002).
[16] A. M. Balagurov *et al.*, Phys. Rev. B **64**, 024420 (2001).
[17] K. Miyano *et al.*, Phys. Rev. Lett. **78**, 4257 (1997).
[18] A. Soibel *et al.*, Nature (London) **406**, 282 (2000).
[19] M. Yasugaki *et al.*, Phys. Rev. B **65**, 212502 (2002).
[20] T. Tamegai *et al.*, in *Magneto-Optical Imaging*, edited by T. H. Johansen and D. V. Shantsev (Kluwer Academic Publishers, Dordrecht, 2004), p. 95.
[21] B. J. Roth, N. G. Sepulveda, and J. P. Wikswo, Jr., J. Appl. Phys. **65**, 361 (1989).
[22] A. Asamitsu *et al.*, Nature (London) **388**, 50 (1997).
[23] V. Kiryukhin *et al.*, Phys. Rev. B **63**, 024420 (2000).
[24] D. Akahoshi *et al.*, Phys. Rev. Lett. **90**, 177203 (2003).
[25] Y. Tomioka *et al.*, Phys. Rev. B **68**, 094417 (2003).
[26] T. Kimura *et al.*, Phys. Rev. Lett. **83**, 3940 (1999).
[27] Y. Okimoto *et al.*, Appl. Phys. Lett. **80**, 1031 (2002).